SCIENTIFIC REPORTS

OPEN

SUBJECT AREAS:
NATURAL PRODUCTS
DRUG REGULATION
BIOCHEMICAL NETWORKS
REGULATORY NETWORKS

Received
15 May 2014

Accepted
26 August 2014

Published
17 September 2014

Correspondence and requests for materials should be addressed to P.-M.Y. (yangpm@tmu.edu.tw)

A gene expression signature-based approach reveals the mechanisms of action of the Chinese herbal medicine berberine

Kuen-Haur Lee, Hsiang-Ling Lo, Wan-Chun Tang, Heidi Hao-yun Hsiao & Pei-Ming Yang

The Ph.D. Program for Cancer Biology and Drug Discovery, College of Medical Science and Technology, Taipei Medical University, Taipei, Taiwan.

Berberine (BBR), a traditional Chinese herbal medicine, was shown to display anticancer activity. In this study, we attempted to provide a global view of the molecular pathways associated with its anticancer effect through a gene expression-based chemical approach. BBR-induced differentially expressed genes obtained from the Gene Expression Omnibus (GEO) at the National Center for Biotechnology Information (NCBI) were analyzed using the Connectivity Map (CMAP) database to compare similarities of gene expression profiles between BBR and CMAP compounds. Candidate compounds were further analyzed using the Search Tool for Interactions of Chemicals (STITCH) database to explore chemical-protein interactions. Results showed that BBR may inhibit protein synthesis, histone deacetylase (HDAC), or AKT/mammalian target of rapamycin (mTOR) pathways. Further analyses demonstrated that BBR inhibited global protein synthesis and basal AKT activity, and induced endoplasmic reticulum (ER) stress and autophagy, which was associated with activation of AMP-activated protein kinase (AMPK). However, BBR did not alter mTOR or HDAC activities. Interestingly, BBR induced the acetylation of α-tubulin, a substrate of HDAC6. In addition, the combination of BBR and SAHA, a pan-HDAC inhibitor, synergistically inhibited cell proliferation and induced cell cycle arrest. Our results provide novel insights into the mechanisms of action of BBR in cancer therapy.

Berberine (BBR) is an isoquinoline alkaloid isolated from various medicinal herbs such as *Coptis chinensis*. It has a long history of use for treating diarrhea in traditional Chinese medicine. BBR was demonstrated to exhibit a wide range of pharmacological actions including anticancer, anti-microbial, anti-inflammatory, and anti-diabetic effects[1]. The anticancer effect of BBR is associated with anti-proliferation, anti-invasion, and apoptosis induction in many tumor cell types[2–6]. In addition to its anticancer activity, novel therapeutic targets of BBR have been extensively investigated[1]. For example, BBR was found to activate AMP-activated protein kinase (AMPK), which has beneficial effects on metabolically disordered states of diabetes[7]. The effects of BBR of inducing apoptosis and inhibiting cancer cell migration and metastasis are also associated with AMPK activation[8–10].

Acetylation and deacetylation of histones play important roles in transcriptional regulation of eukaryotic cells[11]. Histone acetyltransferases (HATs) add acetyl groups to lysine residues and promote a more-relaxed chromatin structure, allowing transcriptional activation. In addition to removing the acetyl group from histone and making the chromatin structure more compact to ultimately silence genes, histone deacetylases (HDACs) also have many non-histone protein substrates such as transcriptional factors, steroid receptors, chaperone proteins and cytoskeletal proteins[12,13]. Overexpression of HDACs was found in tumors, and this inhibits expressions of tumor suppressor genes. Therefore, inhibition of HDACs is considered a potential strategy for treating cancers. However, only two HDAC inhibitors, vorinostat (suberoylanilide hydroxamic acid; SAHA) and romidepsin (depsipeptide or FK228), have been approved by the US Food and Drug Administration (FDA) for treating relapsed cutaneous T-cell lymphoma[14,15].

The Connectivity MAP (CMAP) is a collection of gene-expression profiles from cultured human cells treated with small bioactive molecules, together with pattern-matching software to mine these data. By comparing gene-expression signatures, this tool can be used to find connections among small molecules sharing a mechanism of

Table 1 | Expression signatures of compounds most positively (enrichment score > 0; $p < 0.001$) and negatively (enrichment score < 0; $p < 0.001$) correlated with the gene signature of BBR

Rank	CMAP drug	Function	Mean score	No of instances	Enrichment	p value	Specificity	Percent non-null
1	cycloheximide	protein synthesis inhibitor	0.793	4	0.953	0	0.0226	100
2	trichostatin A	HDAC inhibitor	0.536	182	0.719	0	0.0569	93
3	alvespimycin	HSP90 inhibitor	−0.415	12	−0.655	0	0.0145	75
4	monorden	HSP90 inhibitor	−0.452	22	−0.63	0	0	77
5	tanespimycin	HSP90 inhibitor	−0.431	62	−0.611	0	0.0084	74
6	geldanamycin	HSP90 inhibitor	−0.425	15	−0.608	0	0.0391	73
7	sirolimus	mTOR inhibitor	0.222	44	0.411	0	0.1386	50
8	quinostatin	mTOR inhibitor	0.867	2	0.997	0.00002	0	100
9	vorinostat	HDAC inhibitor	0.446	12	0.638	0.00006	0.2663	75
10	helveticoside	cardiac glycoside	0.684	6	0.807	0.00008	0.034	83
11	thioridazine	calmodulin inhibitor	0.306	20	0.516	0.00008	0.2237	50
12	mycophenolic acid	immunosuppressant	−0.683	3	−0.953	0.00022	0	100
13	0317956-0000	N/A	−0.261	8	−0.692	0.00022	0.0226	50
14	deptropine	antihistamine	0.519	4	0.882	0.00026	0	100
15	iobenguane	radiopharmaceutical	−0.389	4	−0.868	0.0006	0	100
16	digoxigenin	fluorescent probe	0.597	5	0.786	0.00098	0.0263	80
17	norcyclobenzaprine	metabolite of cyclobenzaprine (muscle relaxant)	0.485	4	0.833	0.00117	0.0164	100
18	0297417-0002B	N/A	0.561	3	0.895	0.00226	0.0316	100
19	nifuroxazide	nitrofuran antibiotic	0.561	4	0.799	0.00306	0.0292	100
20	beta-escin	natural triterpenoid saponin	0.316	6	0.673	0.00336	0.0419	66
21	pyrantel	antinematodal thiophene	−0.305	5	−0.718	0.00385	0.0162	60
22	cromoglicic acid	mast cell stabilizer	−0.546	2	−0.954	0.00453	0.0111	100
23	16-phenyl-tetranorprostaglandin E2	N/A	−0.426	4	−0.782	0.00454	0.0119	75
24	streptomycin	antimycobacterial drug; protein synthesis inhibitor	−0.365	4	−0.78	0.00483	0.0061	75
25	lanatoside C	cardiac glycoside	0.383	6	0.643	0.00606	0.2431	50
26	MS-275	HDAC inhibitor	0.611	2	0.938	0.00755	0.1039	100
27	gentamicin	aminoglycoside antibiotic; protein synthesis inhibitor	0.392	4	0.746	0.00792	0.025	100
28	pyrimethamine	antimalarial drug	0.43	5	0.674	0.00965	0.037	80

action, chemical and physiological processes, and diseases and drugs[16]. Because most CMAP compounds are FDA-approved drugs, CMAP has become a powerful tool for drug discovery. The current version (build 02) of CMAP contains more than 7000 expression profiles representing 1309 compounds. By querying CMAP with a gene expression profile of interest and comparing its similarity with CMAP compounds, a list of ranked drugs is obtained. Drugs with negative scores (opposite profiles) may have the potential for treating specific diseases, whereas drugs with positive scores (similar profiles) may be useful for discovering action mechanisms of a drug[17–20].

In this study, we mined the CMAP database to explore the molecular mechanisms of BBR. We present novel functions of BBR of being able to inhibit protein synthesis and AKT activity, and induce ER stress and autophagy. In addition, BBR induced the acetylation of α-tubulin, a substrate of HDAC6, although it did not directly inhibit HDAC activity. Further studies demonstrated that a combination of BBR and SAHA exhibited a synergistic effect on inhibiting cell proliferation and inducing cell cycle arrest in human breast cancer cells. Our results provide a novel view of the anticancer mechanisms of BBR.

Results

A gene expression signature-based approach predicts potential molecular targets of BBR. The CMAP database was used to explore the mechanisms of action of BBR. Differentially expressed genes were prepared from the public microarray data of BBR-treated HepG2 cells[21]. As shown in Supplementary Table S1, 54 genes were upregulated and 7 genes were downregulated by BBR treatment (40 μM for 4 h). This gene set was queried using CMAP, and results are listed in Table 1 according to the given rank. CMAP drugs with positive mean scores (marked in red) had similar gene expression profiles with BBR. The most similar drug to BBR was cycloheximide, a protein synthesis inhibitor. Other major drugs belong to mTOR or HDAC inhibitors. These drugs were further queried using the STTICH database[22] to explore their interactions with proteins (Supplementary Figure S1). These analyses revealed that BBR may inhibit protein synthesis, AKT/mTOR, or HDACs.

BBR inhibits protein synthesis/cell viability and induces eIF2α phosphorylation/autophagy. The anticancer activity of BBR against an MDA-MB-231 human breast cancer cell line was first determined. MDA-MB-231 cells were treated with BBR for 6 ∼ 72 h, and then an MTT assay was performed. As shown in Figure 1a, BBR inhibited cell viability in dose- and time-dependent manners. Because the highest ranked compound in the CMAP analysis was the protein synthesis inhibitor, cycloheximide, we then examined whether BBR reduced protein synthesis. MDA-MB-231 cells were treated with BBR for 6 ∼ 48 h, and equal numbers of cells were harvested and lyzed, and then protein concentration was determined by a Bio-Rad protein assay. As shown in Figure 1b and 1c, BBR treatment for 6 and 24 h did not significantly reduce the protein level. BBR treatment for 48 h inhibited 20.25 ± 1.13% of protein synthesis (Figure 1c), which was associated with a 23.06 ± 6.04% reduction of cell viability by BBR (Figure 1a). Therefore, loss of cell viability may contribute to the inhibition of global protein synthesis by BBR.

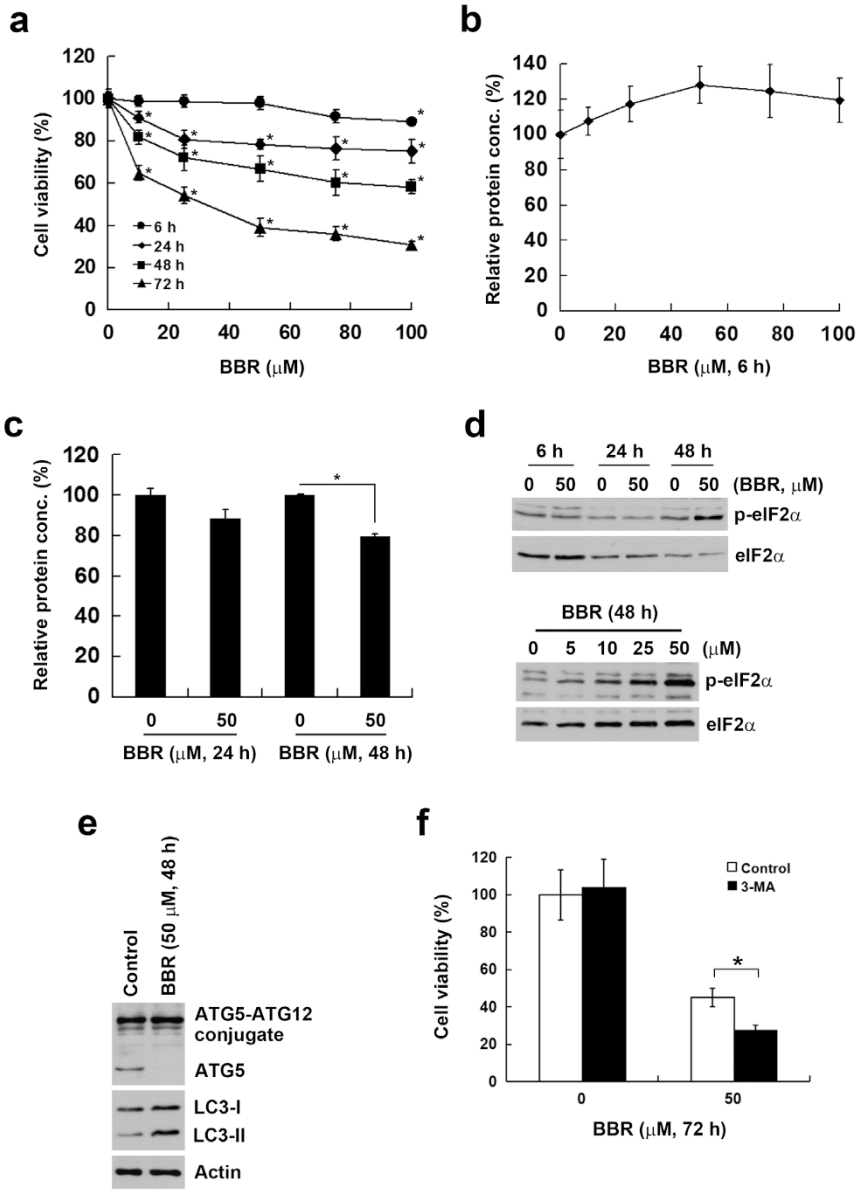

Figure 1 | Effect of BBR on cell viability, protein synthesis, eIF2α phosphorylation, and autophagy. (a) MDA-MB-231 cells were treated with the indicated doses of BBR for 6 ~ 72 h. Cell viability was measured with an MTT assay. (b) MDA-MB-231 cells were treated with the indicated doses of BBR for 6 h, and cells were harvested to prepare total cell lysates. The protein concentration was determined by a Bio-Rad Protein Assay. (c) MDA-MB-231 cells were treated with 50 μM BBR for 24 and 48 h, and cells were harvested to prepare total cell lysates. The protein concentration was determined by a Bio-Rad Protein Assay. (d) MDA-MB-231 cells were treated with 50 μM BBR for 6 ~ 48 h or various doses of BBR for 48 h, and protein expressions of p-eIF2α and eIF2α were analyzed by Western blotting. Images of each indicated probe were cropped from the same blot. (e) MDA-MB-231 cells were treated with 50 μM BBR for 48 h and the protein expressions of ATG5, LC3 and Actin were analyzed by Western blotting. Images of each indicated probe were cropped from the same blot. (f) MDA-MB-231 cells were treated with 50 μM BBR for 72 h in the presence and absence of 1 mM 3-MA. Cell viability was measured with an MTT assay.

Phosphorylation of the alpha subunit of eIF2 (eIF2α) at serine-51 is one of the best-characterized mechanisms for downregulating protein synthesis in higher eukaryotes in response to various stress conditions[23]. We found that BBR treatment at 48 h induced eIF2α phosphorylation (Figure 1d). Therefore, BBR inhibited global protein synthesis, which is associated with eIF2α phosphorylation. Phosphorylation of eIF2α is also a well-known marker of endoplasmic reticulum (ER) stress and was reported to connect ER stress to autophagy[24]. To investigate whether BBR also induced autophagy, LC3 expression was examined by a Western blot analysis. Two forms of LC3, including cytosolic LC3-I (autophagy-inactive) and processed LC3-II (autophagy-active), exist. During autophagy, LC3-I is converted into LC3-II. Because LC3-II is localized in autophagosome membranes, the level of LC3-II expression is proportional to that of autophagy[25]. As shown in Figure 1e, BBR induced LC3-II accumulation. Autophagy-related protein 5 (ATG5), an E3 ubiquitin ligase, is known to initiate the formation of autophagosomes[26]. The covalent binding of ATG12 to ATG5 through an ubiquitin-like conjugation system further promotes the elongation of autophagosomes and the conversion of LC3[27]. We found that the free form of ATG5 decreased upon BBR treatment (Figure 1f). To investigate the effects of autophagy on the anticancer activity of BBR, MDA-MB-231 cells were treated with BBR in the presence and absence of 3-methyladenine (3-MA), and an MTT assay was subsequently performed. 3-MA,

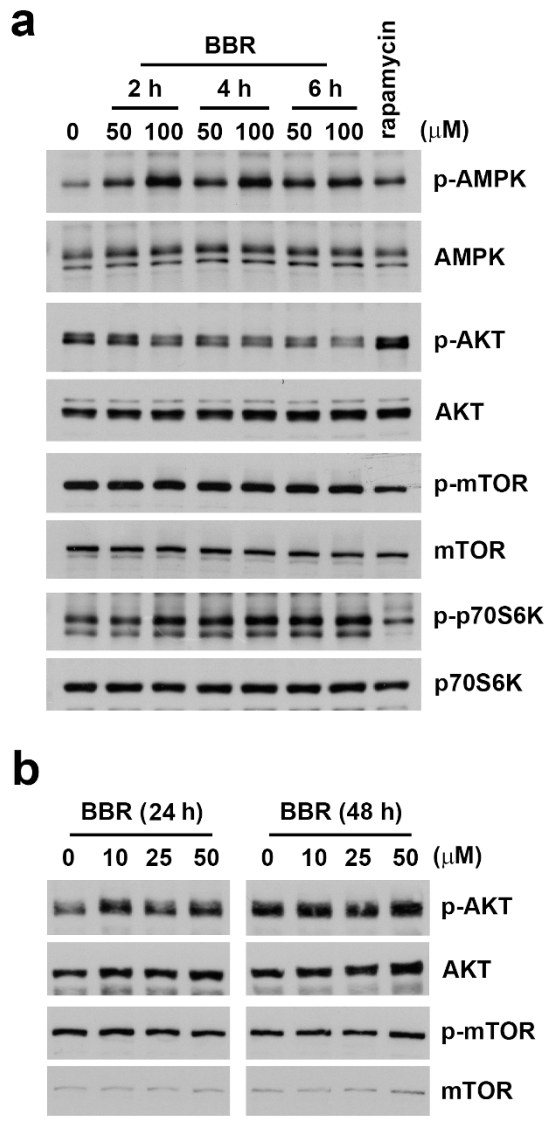

Figure 2 | Effect of BBR on AMPK and AKT/mTOR/p70S6K activities. (a) MDA-MB-231 cells were treated with 50 or 100 μM BBR for 2 ~ 6 h or 5 μM rapamycin for 6 h. Protein expressions of p-AMPK, AMPK, p-AKT, AKT, p-mTOR, mTOR, p-p70S6K, and p70S6K were analyzed by Western blotting. Images of each indicated probe were cropped from the same blot. (b) MDA-MB-231 cells were treated with various doses of BBR for 24 or 48 h or 5 μM rapamycin for 6 h. Protein expressions of p-AKT, AKT, p-mTOR, and mTOR were analyzed by Western blotting. Images of each indicated probe were cropped from the same blot.

a class III PI3K inhibitor, was found to block autophagosome formation in the early stage of autophagy[25], and BBR-induced cytotoxicity was augmented by 3-MA (Figure 1f). Therefore, BBR induced cytoprotective autophagy.

BBR activates AMPK and inhibits basal AKT activity. Inhibition of mTOR signaling is known to stimulate autophagy[28]. AMPK induces autophagy through phosphorylation and activation of the TSC1/TSC2 complex, a negative regulator of mTOR[29,30]. In contrast, AKT phosphorylates and activates mTOR to suppress autophagy[31]. Because BBR is a strong inducer of AMPK[7], we hypothesized that BRR might induce autophagy through altering these signaling pathways. Activation of AMPK induced by BBR treatment was confirmed by its phosphorylation at Thr172 (Figure 2a). However, phosphorylation of mTOR did not change in response to BBR treatment, although BBR reduced the level of AKT phosphorylation (Figure 2a). Interestingly, the activity of p70S6K, a downstream substrate of mTOR, was induced by BBR (Figure 2a). However, rapamycin, a well-known mTOR inhibitor, inhibited the phosphorylation of both mTOR and p70S6K (Figure 2a). Moreover, long-term (24 and 48 h) treatment with BBR did not alter the levels of either AKT or mTOR phosphorylation (Figure 2a). These results suggest that BBR transiently activates AMPK and inhibits AKT, but does not inhibit mTOR activity.

Molecular docking analyses of BBR to HDACs. The result of the CMAP analysis also revealed that HDACs are possible targets of BBR. A previous study using *in silico* docking showed that BBR interacts with HDAC1 and HDAC3 with respective binding energies of −5.7 and −6.37 kcal/mol, which are comparable to the well-known HDAC inhibitor, trichostatin A (TSA), that exhibits binding energies of −6.89 kcal/mol with HDAC1 and −6.41 kcal/mol with HDAC3[32]. There are 18 HDACs identified in humans. They are classified based on homologies to yeast HDACs[11,33]. Classes I (HDACs 1, 2, 3 and 8), IIa (HDACs 4, 5, 7 and 9), IIb (HDACs 6 and 10), and IV (HDAC11) are zinc-dependent deacetylases[11,33]. Class III HDACs (sirtuins 1 ~ 7) are zinc-independent and require NAD^+ for their activities[34]. To gain more insights into the binding of BBR with different classes of zinc-dependent HDACs, we performed molecular docking analyses of BBR to HDAC2 (class I), HDAC8 (class I), HDAC4 (class IIa), HDAC7 (class IIa), and HDAC6 (class IIb). In addition, the FDA-approved HDAC inhibitor, SAHA, was also docked with these HDACs as a reference compound. As shown in Supplementary Figure S2, BBR interacted with HDACs through its methylenedioxyphenyl moiety. The total fitness energies of BBR binding to HDACs (except for HDAC7) were lower than those of SAHA (Supplementary Table S2). In addition, the energies of hydrogen bond formation of BBR-HDACs were much weaker than those of SAHA (Supplementary Table S2). Therefore, the interaction profiles possibly imply that BBR is not a potential HDAC inhibitor.

BBR induces the acetylation of α-tubulin. To investigate whether BBR directly inhibits HDAC activity, an *in vitro* colorimetric assay was performed. Whole-cell lysates of MDA-MB-231 cells were incubated with various doses of BBR or 5 μM SAHA for 1 h, and then the substrates were added and incubated for an additional 2 h. As shown in Figure 3a, SAHA but not BBR inhibited HDAC activity, suggesting that BBR is not an HDAC inhibitor. Interestingly, a Western blot analysis showed that BBR induced the acetylation of α-tubulin although the acetylation of histone H3 was not altered (Figure 3b). α-Tubulin is a well-known substrate of HDAC6 that is frequently localized in the cytosol[35]. Therefore, we further examined the localization of BBR-induced α-tubulin acetylation by nuclear and cytosolic fractionation. As shown in Figure 3c, acetylation of histone H3 and localization of HDAC1 and HDAC2 were not altered by BBR. Interestingly, the acetyl-α-tubulin was predominant in nuclei, which was not due to different localizations of α-tubulin and HDAC6.

Anti-proliferation and anti-migration effects of BBR and SAHA toward MDA-MB-231 cells. To investigate whether SAHA can enhance BBR-induced growth inhibition, MDA-MB-231 cells were treated with various doses of BBR for 72 h in the presence and absence of 2 μM SAHA, and then an MTT assay was performed. As shown in Figure 4a, SAHA potentiated the anti-proliferative effect of BBR. To examine whether the anti-proliferative effects of BBR and SAHA resulted from induction of apoptosis, cleavage of poly (ADP-ribose) polymerase (PARP) was analyzed by western blotting. PARP, a 116-kDa enzyme involved in DNA repair and maintenance of genomic integrity, is cleaved into 24- and 89-kDa fragments by active caspase-3 during the early phases of apoptosis[36]. As shown in Figure 4b, doxorubicin was used as a positive control and it induced PARP cleavage. However, PARP was not cleaved by BBR,

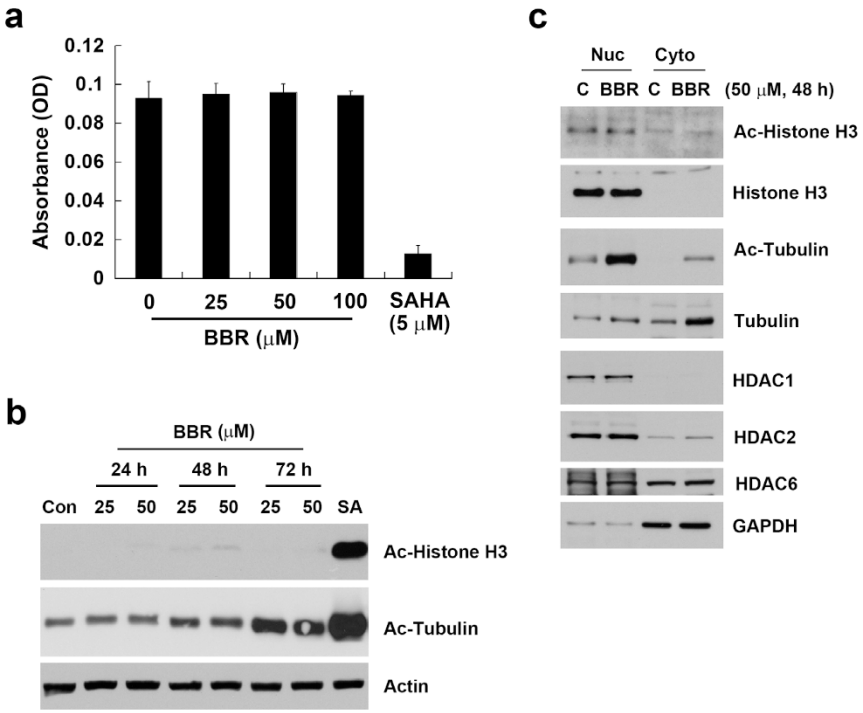

Figure 3 | Effect of BBR on HDAC activity and acetylation of histone H3 and α-tubulin. (a) Total cells lysates were incubated with various doses of BBR or 5 μM SAHA in HDAC assay buffer for 3 h. HDAC activity was initiated by adding the HDAC substrate and incubating at 37°C for 1 h. HDAC activity was measured by detecting the OD value at 405 nm. (b) MDA-MB-231 cells were treated with 25 or 50 μM BBR for 24 ~ 72 h or 1 μM SAHA for 24 h. Protein expressions of Ac-histone H3, Ac-α-tubulin and β-actin were analyzed by Western blotting. Images of each indicated probe were cropped from the same blot. (c) MDA-MB-231 cells were treated with 50 μM BBR for 48 h, and nuclear and cytosolic extracts were prepared as described in "Methods". Protein expressions of Ac-histone H3, histone H3, Ac-α-tubulin, α-tubulin, HDAC1, HDAC2, HDAC6, and GAPDH were analyzed by Western blotting. Images of each indicated probe were cropped from the same blot.

SAHA, or their combination, suggesting that BBR/SAHA did not induce apoptosis. To further confirm this result, a flow cytometric analysis was performed to examine levels of cell proliferation, DNA damage, and apoptosis by 5-bromodeoxyuridine (BrdU) incorporation, γH2AX (phosphorylation of H2AX), and cleaved PARP staining, respectively. BrdU, an analog of the DNA precursor, thymidine, can be incorporated into newly synthesized DNA, which serves as an index of cell proliferation[37]. H2AX, a member of the histone H2A protein family, is rapidly phosphorylated at serine-139 when DNA strand breaks occur. γH2AX can recruit DNA damage repair proteins to the site of DNA damage[38]. As shown in Figure 4c, neither BBR, SAHA, nor their combination altered levels of γH2AX and cleaved PARP. However, BBR or SAHA alone reduced the level of BrdU incorporation, which was further enhanced by their combination (Figure 4c). These results showed that the anticancer effect of BBR and/or SAHA resulted from inhibition of cell proliferation. To further investigate whether BBR and/or SAHA disturbed progression of the cell cycle, a flow cytometric analysis was performed with propidium iodide (PI) staining. Consistently, BBR or SAHA alone induced G_2 arrest, which was enhanced by their combination (Figure 4d). Because α-tubulin deacetylation was found to enhance cell motility through a reduction in microtubule stability[35], BBR may inhibit cell migration through the increased acetylation of α-tubulin. To investigate this possibility, a wound-healing assay was performed. As shown in Figure 5, BBR alone inhibited cell migration. However, the combination of BBR and SAHA did not further reduce migrating cells.

Discussion

Natural compounds derived from plants have long been used to treat a number of human diseases. Among them, BBR has been employed in Ayurvedic and Chinese medicine for hundreds of years with a wide range of pharmacological and biochemical effects. Growing evidence supports BBR exhibiting anticancer effects[1]. However, the underlying molecular mechanisms are not well understood. A CMAP analysis provides a powerful strategy because gene expression signatures of a drug candidate can be used to query the CMAP database and explore connections with existing drugs[16]. For example, the natural compounds, celastrol and gedunin, were found to act as HSP90 inhibitors by a CMAP analysis[19]. In this study, we found that the gene expression signature of BBR was positively correlated with that of protein synthesis, AKT/mTOR, and HDAC inhibitors. Further studies confirmed that BBR inhibited global protein synthesis and basal AKT activity, as well as induced the acetylation of α-tubulin in human breast cancer cells. Our results provide a global view of the mechanisms of action of BBR.

Breast cancer is the most common cancer among women worldwide, and development of novel therapeutic agents is urgently needed. Although BBR is regarded as a potential therapeutic drug for breast cancer, a better understanding of genes and cellular pathways regulated by BBR is needed to define the mechanisms of its action in cancer treatment[39]. A recent study also performed genome-wide expression profiling of BBR-treated human breast cancer cells (MCF-7 and MDA-MB-231 cells) using complementary DNA (cDNA) microarrays[40]. This study identified that many of the target genes of BBR are involved in regulating the cell cycle and cell migration[40], which is comparable to our findings. Another study employed proteomic strategy to identify the molecular targets of BBR in MCF-7 cells[41]. This study revealed that BBR downregulates the majority (63%) of identified proteins involving in protein folding, redox regulation, gene regulation and signal transduction[41]. BBR reduces the expression of chaperone and folding proteins such as heat shock protein 90 (HSP90), 78 kDa glucose-regulated protein (GRP78)

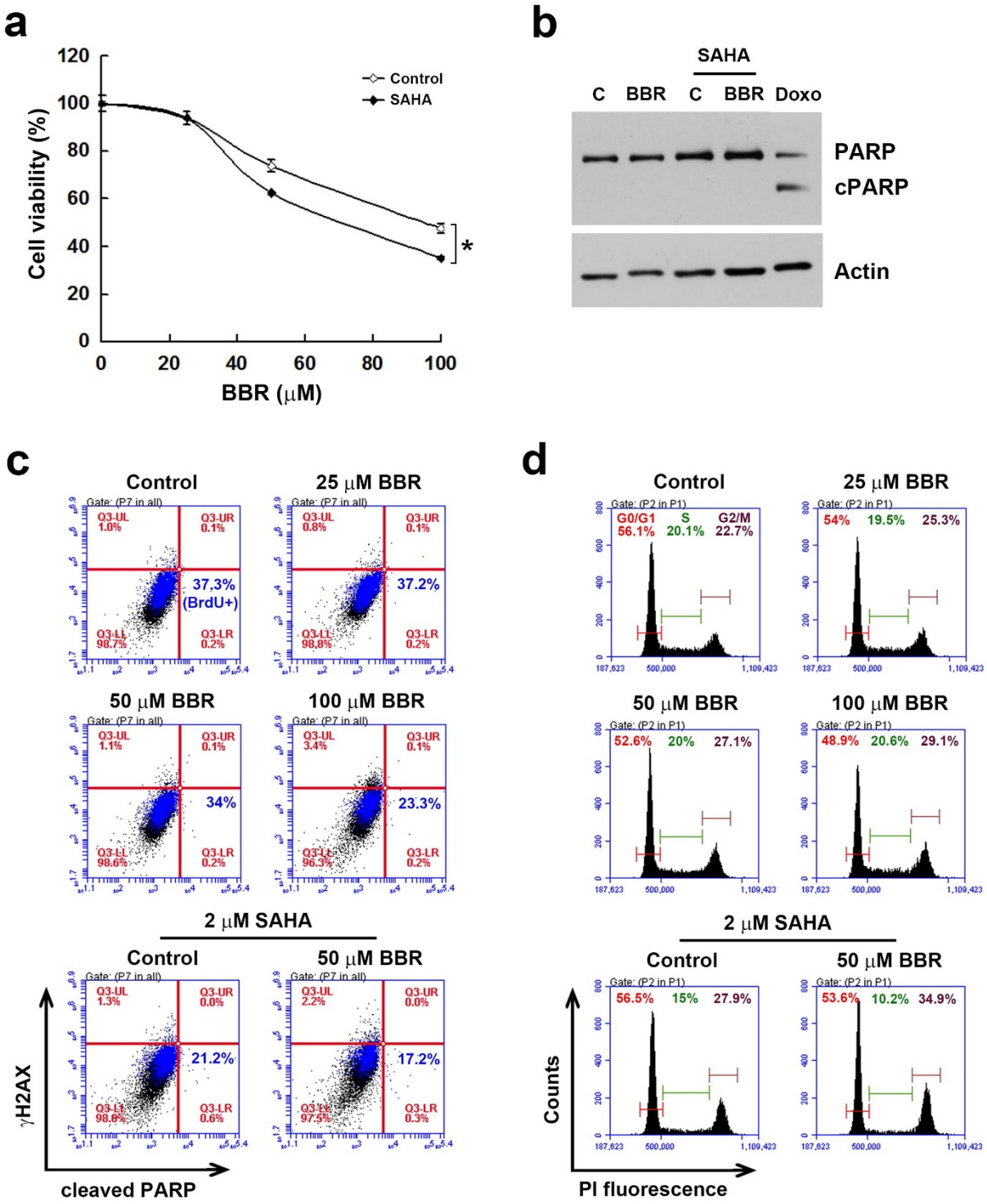

Figure 4 | Effect of BBR on cell viability, cell cycle, apoptosis, DNA damage, and cell proliferation. (a) MDA-MB-231 cells were treated with various doses of BBR for 72 h in the presence and absence of 2 μM SAHA. Cell viability was measured with an MTT assay. (b) MDA-MB-231 cells were treated with 50 μM BBR for 72 h in the presence and absence of 2 μM SAHA, or with 0.75 μM doxorubicin (Doxo) for 72 h. Protein expressions of PARP, cleaved PARP (cPARP), and β-actin were analyzed by Western blotting. Images of each indicated probe were cropped from the same blot. (c) MDA-MB-231 cells were treated with various doses of BBR for 48 h in the presence and absence of 2 μM SAHA. Apoptosis, DNA damage, and cell proliferation were examined as described in "Methods". (d) MDA-MB-231 cells were treated with various doses of BBR for 48 h in the presence and absence of 2 μM SAHA. The cell cycle was analyzed by flow cytometry.

and peptidylprolyl isomerase A (PPIA/cyclophilin A)[41], which may contribute to the inhibition of global protein synthesis as observed in our study.

In addition to the gene expression signature-based approach used in this study, there are different ways that can be used to predict the mechanisms of action of BBR. For example, the network pharmacology approach has been successfully used to evaluate several herbal formulae and compounds[42–45]. Many therapeutic drugs usually exhibit actions on more than one molecular target, which is a phenomenon known as polypharmacology[46]. Network pharmacology

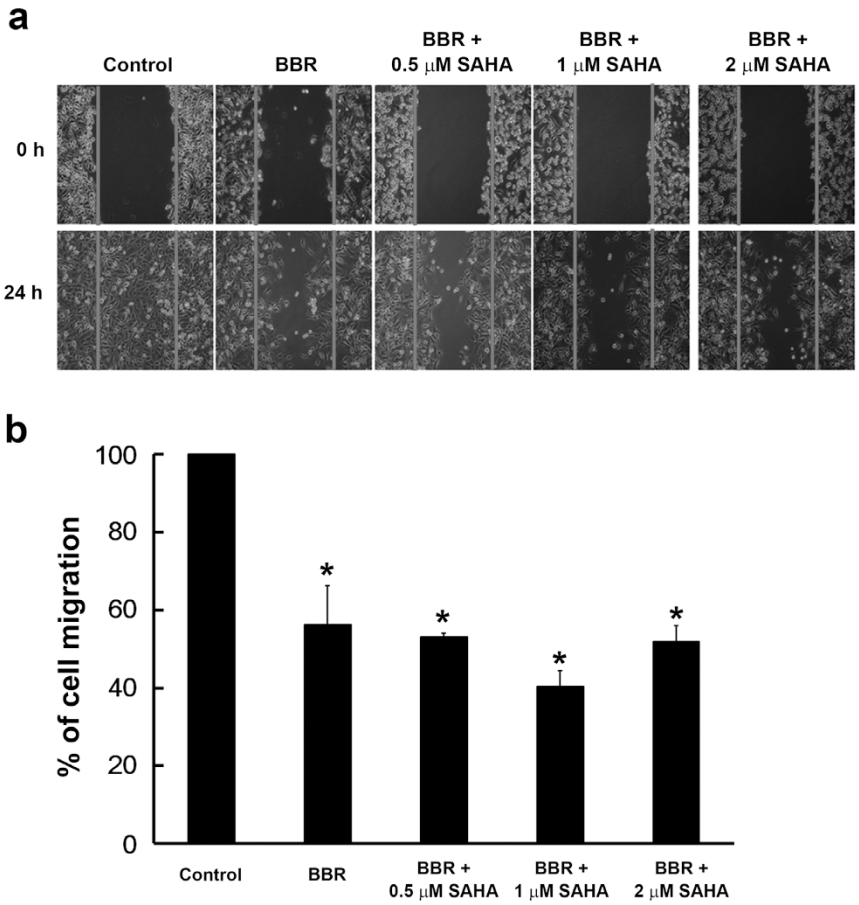

Figure 5 | Effect of BBR on cell migration. MDA-MB-231 cells were treated with 50 μM BBR for 48 h. Cells were trypsinized, spread on 6-well plates, and treated with various doses of SAHA for an additional 24 h. Cell migration was analyzed by a wound-healing assay as described in ''Methods''. Photographs at times = 0 and 24 h are shown in (a). Percentages of migrating cells are shown in (b).

applies systems biology and network analysis to drugs and drug targets through integration of not only gene expression profiles, but also metabolomics and protein-protein interactions[47,48]. Therefore, it would be worth performing network pharmacology-based predictions for BBR to gain more insights into the mechanisms of its action and accelerate its application.

It is surprising that the most similar drug to BBR was cycloheximide, an inhibitor of protein synthesis. Cycloheximide inhibits transfer of amino acid from soluble RNA to polypeptide, thus blocking translation elongation[49]. BBR has been reported to interact with poly(A) mRNA and tRNA[50], which may cause inhibition of transcriptional and translational activities. However, our results show that inhibition of global protein synthesis by BBR was associated with the loss of cell viability. Further investigations using more specific assays, such as pulse-chased labeling with [35S]-methionine, are needed to clarify the effect of BBR on nascent protein synthesis.

An interesting finding of this study was that BBR induced the acetylation of α-tubulin, particular in nuclei, without disturbing histone H3 acetylation, which is consistent with a previous study conducted on HL-60 human promyelocytic cells[51]. It was found that microtubules contain acetylated α-tubulin in mammalian cells, and the amount of acetylated α-tubulin is thought to be proportional to the stability of microtubules. In addition, taxol, a microtubule-stabilizing agent, induces the acetylation of α-tubulin[52,53]. Therefore, α-tubulin may be a direct target of BBR. Indeed, target predictions for BBR through the ChEMBL website (European Bioinformatics Institute) indicated that α/β-tubulins are possible targets of BBR (Supplementary Table S3), which warrants further investigation in the future.

Our previous study found that SAHA induces autophagy that potentiates its anticancer action against hepatocellular carcinoma[54]. However, statins, 3-hydroxy-3-methylglutaryl-CoA reductase inhibitors with cholesterol-lowering properties, exhibit HDAC-inhibitory activity and induce cytoprotective autophagy[55]. According to those two studies, we propose a working model to explain the role of autophagy in cell fate decisions in response to SAHA and statins[56]. Statins induce AMPK activation and cytosolic p21 expression, leading to ER stress and cytoprotective autophagy[55,56]. In contrast, HDAC inhibitors induce autophagic cell death through inhibition of AKT/mTOR signaling, which is not dependent on AMPK or p21[54,56]. Because BBR is a strong inducer of AMPK[7], we hypothesized that BRR might induce cytoprotective autophagy through the mode of statins. Indeed, BBR induced ER stress and cytoprotective autophagy in MDA-MB-231 cells. In addition, BBR failed to induce p21 expression (data not shown), which was probably due to the fact that MDA-MB-231 cells express a mutant form of p53[57]. Although BBR inhibited the basal activity of AKT, it did not alter the activity of mTOR. Therefore, BBR might induce cytoprotective autophagy through AMPK- and ER stress-dependent pathways, which is similar to the mechanism of statins.

One limitation of this study was the use of gene expression profiles from BBR-treated HepG2 cells. The CMAP contains microarray datasets from 4 cancer cell lines (MCF-7 breast cancer, PC-3 prostate cancer, HL-60 leukemia and SKMEL5 melanoma). It is postulated that disease-associated gene signatures can be compared to the CMap drug signature profiles to reveal potential drug lists despite the profiles being of different cell lines[16]. However, we still cannot exclude the possibility that variations derived from different cell

types, experimental conditions and platforms may occur. For example, BBR was shown to inhibit mTOR activity through down-regulating AKT or activating AMPK activity in HepG2 cells[58,59], which confirms the results of the predictions in this study. In contrast, we found that BBR did not alter mTOR activity in MDA-MB-231 cells, suggesting that a cell type-specific effect of BBR indeed exists.

In conclusion, we report how integrative gene expression-based chemical genomics can be useful for discovering the mechanisms of action of a drug. Our results may provide novel molecular insights into the anticancer mechanisms of BBR.

Methods

Materials. Dulbecco's modified Eagle's medium (DMEM), L-glutamine, sodium pyruvate, and Antibiotic-Antimycotic (penicillin G, streptomycin and amphotericin B) were purchased from Life Technologies. Fetal bovine serum (FBS) was purchased from Biological Industries. Antibodies specific for β-actin (GTX109639; 1 : 15000), AKT1 (GTX110613; 1 : 7500), phospho-Thr308-AKT1 (GTX61798; 1 : 500), AMPKα1 (GTX112998; 1 : 5000), phospho-Thr172-AMPKα (GTX63165; 1 : 2000), ATG5 (GTX113309; 1 : 2500), eIF2α (GTX101241; 1 : 250), phospho-Ser51-eIF2α (GTX50300; 1 : 1500), GAPDH (GTX100118; 1 : 30000), HDAC1 (GTX100513; 1 : 5000), HDAC2 (GTX109642; 1 : 5000), HDAC6 (GTX100722; 1 : 10000), histone H3 (GTX122148; 1 : 1000), acetyl-histone H3 (GTX122648; 1 : 5000), LC3B (GTX127375; 1 : 10000), mTOR (GTX101558; 1 : 500), phospho-Ser2448-mTOR (GTX62472; 1 : 2000), p70S6K (GTX103174; 1 : 500), phospho-p70S6K (GTX62758; 1 : 1500), and α-tubulin (GTX112141; 1 : 5000) were purchased from GeneTex. PARP1 (#9542S; 1 : 1000) and acetyl-Lys40-α-tubulin (#5335; 1 : 2000) antibodies were purchased from Cell Signaling Technology. Horseradish peroxidase-labeled goat anti-rabbit (111-035-003; 1 : 10000) and anti-mouse (115-035-003; 1 : 10000) secondary antibodies were purchased from Jackson ImmunoResearch. Berberine (BBR), doxorubicin and 3-(4,5-dimethylthiazol-2-yl)-2,5-diphenyl tetrazolium bromide (MTT) were purchased from Sigma. Suberoylanilide hydroxamic acid (SAHA) and 3-methyladenine (3-MA) were purchased from Cayman. Rapamycin was purchased from LC Laboratories. Protease and phosphatase inhibitor cocktails were purchased from Roche.

Cell culture. MDA-MB-231 human breast cancer cells, kindly provided by Prof. Shu-Jun Chiu (Department of Life Sciences, Tzu Chi University, Hualien, Taiwan), were cultured in DMEM supplemented with 10% FBS, 2 mM L-glutamine, 1 mM sodium pyruvate, 100 units/mL penicillin G, 100 μg/mL streptomycin, and 0.25 μg/mL amphotericin B. Cells were cultured at 37°C and 5% CO_2 in a humidified incubator and passaged every 2 or 3 days.

Preparation of total cell lysates, nuclear/cytosol fractionation and determination of protein concentrations. For total cell lysates, cells were lysed in an ice-cold buffer containing 50 mM Tris-HCl (pH 7.5), 150 mM NaCl, 1 mM $MgCl_2$, 2 mM EDTA, 1% NP-40, 10% glycerol, 1 mM DTT, and 1 × protease and phosphatase inhibitor cocktails at 4°C for 30 min. After centrifugation, the supernatants were transferred to new tubes and stored at −20°C. Nuclear and cytosolic extracts was prepared using a Nuclear/Cytosol Fractionation Kit (BioVision) according to the manufacturer's instructions. Protein concentrations were determined with a Bio-Rad Protein Assay.

Western blot analysis. Proteins in the cell lysate (50 μg) were separated on a 10% sodium dodecylsulfate (SDS)-polyacrylamide gel, then transferred electrophoretically onto Hybond-C Extra nitrocellulose membranes (GE Healthcare Life Sciences). Membranes were pre-hybridized in 20 mM Tris-base, 150 mM NaCl, 0.05% Tween-20 (TBST buffer), and 5% skim milk for 1 h, then transferred to a solution containing 1% BSA/TBST and primary antibody and incubated overnight at 4°C. After washing with the TBST buffer, membranes were submerged in 1% BSA/TBST containing a horseradish peroxidase-conjugated secondary antibody for 1 h. Membranes were washed with TBST buffer, then developed using the Western Lightning Plus ECL detecting reagent (PerkinElmer) and exposed to x-ray film (Fujifilm).

Cell viability assay. Cell viability was measured by an MTT assay. Cells were plated in 96-well plates and treated with drugs. After incubation for the indicated time intervals, 0.5 mg/mL of MTT was added to each well for an additional 4 h. The blue MTT formazan precipitate was then dissolved in 200 μL DMSO. The absorbance at 550 nm was measured on a multi-well plate reader.

***In vitro* HDAC activity assay.** The global HDAC activity was determined with an HDAC Activity Colorimetric Assay Kit (BioVision). Incubations were performed at 37°C with total cell extracts, BBR, or SAHA, and the HDAC reaction was initiated by the addition of Ac-Lys(Ac)-pNA substrate. After 3 h, Lysine Developer was added, and the mixture was incubated for another 30 min. The optical density (OD) at 405 nm was measured using a multi-well plate reader. HDAC activity was expressed as the relative OD value.

Flow cytometric analyses of the cell cycle, apoptosis, DNA damage, and cell proliferation. Cells were plated in 6-well plates for 24 h, then treated with complete medium containing drugs for 48 h. Floating and adherent cells were harvested. For the cell cycle analysis, cells were immediately fixed with 75% ethanol and stored at −20°C. Cells were stained in a propidium iodide (PI) staining buffer (10 μg/mL PI and 100 μg/mL RNase A) for 30 min and then analyzed on a BD Accuri C6 flow cytometer. For apoptosis, DNA damage, and cell proliferation determinations, cells were stained with a BD Pharmingen Apoptosis, DNA Damage and Cell Proliferation Kit according to the manufacturer's instructions.

Wound-healing assay. Cells were cultured at a density of 8×10^5 cells per well in 6-well plates for 24 h, resulting in a monolayer at more than 90% confluence. Monolayer cells were scraped with a 200-μL pipette tip to generate a wound and treated with drugs for 24 h. Photographs were taken at 0 and 24 h at the same position of the wound. The average distance of the wound was calculated using Image J software. The ability of cells to close the wound was calculated as follows: 100 × [(surface area of the wound at t = 0 h) − (surface area of the wound at t = 24 h)]/(surface area of the wound at t = 0 h).

Statistical analysis. Data were analyzed using Student's *t*-test, and *p* values of <0.05 were considered significant (*).

1. Tillhon, M., Guaman Ortiz, L. M., Lombardi, P. & Scovassi, A. I. Berberine: new perspectives for old remedies. *Biochem. Pharmacol.* **84**, 1260–1267 (2012).
2. Iizuka, N. *et al.* Inhibitory effect of Coptidis Rhizoma and berberine on the proliferation of human esophageal cancer cell lines. *Cancer Lett.* **148**, 19–25 (2000).
3. Liu, B. *et al.* Berberine inhibits human hepatoma cell invasion without cytotoxicity in healthy hepatocytes. *PLoS One* **6**, e21416 (2011).
4. Mantena, S. K., Sharma, S. D. & Katiyar, S. K. Berberine, a natural product, induces G1-phase cell cycle arrest and caspase-3-dependent apoptosis in human prostate carcinoma cells. *Mol. Cancer Ther.* **5**, 296–308 (2006).
5. Peng, P. L., Hsieh, Y. S., Wang, C. J., Hsu, J. L. & Chou, F. P. Inhibitory effect of berberine on the invasion of human lung cancer cells via decreased productions of urokinase-plasminogen activator and matrix metalloproteinase-2. *Toxicol. Appl. Pharmacol.* **214**, 8–15 (2006).
6. Wang, L. *et al.* Berberine inhibits proliferation and down-regulates epidermal growth factor receptor through activation of Cbl in colon tumor cells. *PLoS One* **8**, e56666 (2013).
7. Lee, Y. S. *et al.* Berberine, a natural plant product, activates AMP-activated protein kinase with beneficial metabolic effects in diabetic and insulin-resistant states. *Diabetes* **55**, 2256–2264 (2006).
8. Kim, H. S. *et al.* Berberine-induced AMPK activation inhibits the metastatic potential of melanoma cells via reduction of ERK activity and COX-2 protein expression. *Biochem. Pharmacol.* **83**, 385–394 (2012).
9. Park, J. J. *et al.* Berberine inhibits human colon cancer cell migration via AMP-activated protein kinase-mediated downregulation of integrin beta1 signaling. *Biochem. Biophys. Res. Commun.* **426**, 461–467 (2012).
10. Yang, X. & Huang, N. Berberine induces selective apoptosis through the AMPKmediated mitochondrial/caspase pathway in hepatocellular carcinoma. *Mol Med Rep* **8**, 505–510 (2013).
11. Lehrmann, H., Pritchard, L. L. & Harel-Bellan, A. Histone acetyltransferases and deacetylases in the control of cell proliferation and differentiation. *Adv. Cancer Res.* **86**, 41–65 (2002).
12. Jenuwein, T. & Allis, C. D. Translating the histone code. *Science* **293**, 1074–1080 (2001).
13. Xu, W. S., Parmigiani, R. B. & Marks, P. A. Histone deacetylase inhibitors: molecular mechanisms of action. *Oncogene* **26**, 5541–5552 (2007).
14. Campas-Moya, C. Romidepsin for the treatment of cutaneous T-cell lymphoma. *Drugs Today (Barc)* **45**, 787–795 (2009).
15. Mann, B. S., Johnson, J. R., Cohen, M. H., Justice, R. & Pazdur, R. FDA approval summary: vorinostat for treatment of advanced primary cutaneous T-cell lymphoma. *Oncologist* **12**, 1247–1252 (2007).
16. Lamb, J. *et al.* The Connectivity Map: using gene-expression signatures to connect small molecules, genes, and disease. *Science* **313**, 1929–1935 (2006).
17. Fayad, W. *et al.* Identification of a novel topoisomerase inhibitor effective in cells overexpressing drug efflux transporters. *PLoS One* **4**, e7238 (2009).
18. Gheeya, J. *et al.* Expression profiling identifies epoxy anthraquinone derivative as a DNA topoisomerase inhibitor. *Cancer Lett.* **293**, 124–131 (2010).
19. Hieronymus, H. *et al.* Gene expression signature-based chemical genomic prediction identifies a novel class of HSP90 pathway modulators. *Cancer Cell* **10**, 321–330 (2006).
20. Wen, Z. *et al.* Discovery of molecular mechanisms of traditional Chinese medicinal formula Si-Wu-Tang using gene expression microarray and connectivity map. *PLoS One* **6**, e18278 (2011).
21. Lo, T. F., Tsai, W. C. & Chen, S. T. MicroRNA-21-3p, a berberine-induced miRNA, directly down-regulates human methionine adenosyltransferases 2A and 2B and inhibits hepatoma cell growth. *PLoS One* **8**, e75628 (2013).
22. Kuhn, M. *et al.* STITCH 4: integration of protein-chemical interactions with user data. *Nucleic Acids Res.* **42**, D401–407 (2014).

23. de Haro, C., Mendez, R. & Santoyo, J. The eIF-2alpha kinases and the control of protein synthesis. *FASEB J.* **10**, 1378–1387 (1996).
24. Hoyer-Hansen, M. & Jaattela, M. Connecting endoplasmic reticulum stress to autophagy by unfolded protein response and calcium. *Cell Death Differ.* **14**, 1576–1582 (2007).
25. Klionsky, D. J. *et al.* Guidelines for the use and interpretation of assays for monitoring autophagy. *Autophagy* **8**, 445–544 (2012).
26. Mizushima, N. *et al.* Dissection of autophagosome formation using Apg5-deficient mouse embryonic stem cells. *J. Cell Biol.* **152**, 657–668 (2001).
27. Mizushima, N. *et al.* A protein conjugation system essential for autophagy. *Nature* **395**, 395–398 (1998).
28. Meijer, A. J. & Dubbelhuis, P. F. Amino acid signalling and the integration of metabolism. *Biochem. Biophys. Res. Commun.* **313**, 397–403 (2004).
29. Inoki, K., Zhu, T. & Guan, K. L. TSC2 mediates cellular energy response to control cell growth and survival. *Cell* **115**, 577–590 (2003).
30. Matsui, Y. *et al.* Distinct roles of autophagy in the heart during ischemia and reperfusion: roles of AMP-activated protein kinase and Beclin 1 in mediating autophagy. *Circ. Res.* **100**, 914–922 (2007).
31. Manning, B. D. & Cantley, L. C. United at last: the tuberous sclerosis complex gene products connect the phosphoinositide 3-kinase/Akt pathway to mammalian target of rapamycin (mTOR) signalling. *Biochem. Soc. Trans.* **31**, 573–578 (2003).
32. Sangeetha, S., Ranjitha, S., Murugan, K. & Kumar, G. R. Breast Cancer Specific Histone Deacetylase Inhibitors and Lead Discovery using Molecular Docking and Descriptor Study. *Trends in Bioinformatics* **6** (2013).
33. Dokmanovic, M., Clarke, C. & Marks, P. A. Histone deacetylase inhibitors: overview and perspectives. *Mol. Cancer Res.* **5**, 981–989 (2007).
34. Sauve, A. A., Wolberger, C., Schramm, V. L. & Boeke, J. D. The biochemistry of sirtuins. *Annu. Rev. Biochem.* **75**, 435–465 (2006).
35. Hubbert, C. *et al.* HDAC6 is a microtubule-associated deacetylase. *Nature* **417**, 455–458 (2002).
36. Krishnakumar, R. & Kraus, W. L. The PARP side of the nucleus: molecular actions, physiological outcomes, and clinical targets. *Mol. Cell* **39**, 8–24 (2010).
37. Li, C. Specific cell cycle synchronization with butyrate and cell cycle analysis. *Methods Mol. Biol.* **761**, 125–136 (2011).
38. Kuo, L. J. & Yang, L. X. Gamma-H2AX - a novel biomarker for DNA double-strand breaks. *In Vivo* **22**, 305–309 (2008).
39. Jabbarzadeh Kaboli, P., Rahmat, A., Ismail, P. & Ling, K. H. Targets and mechanisms of berberine, a natural drug with potential to treat cancer with special focus on breast cancer. *Eur. J. Pharmacol.* **740C**, 584–595 (2014).
40. Wen, C. J. *et al.* Genomic screening for targets regulated by berberine in breast cancer cells. *Asian Pac. J. Cancer Prev.* **14**, 6089–6094 (2013).
41. Chou, H. C. *et al.* Proteomic and redox-proteomic analysis of berberine-induced cytotoxicity in breast cancer cells. *J. Proteomics* **75**, 3158–3176 (2012).
42. Li, S., Zhang, B., Jiang, D., Wei, Y. & Zhang, N. Herb network construction and co-module analysis for uncovering the combination rule of traditional Chinese herbal formulae. *BMC Bioinformatics* **11 Suppl 11**, S6 (2010).
43. Liang, X., Li, H. & Li, S. A novel network pharmacology approach to analyse traditional herbal formulae: the Liu-Wei-Di-Huang pill as a case study. *Mol Biosyst* **10**, 1014–1022 (2014).
44. Zhang, B. *et al.* Vitexicarpin acts as a novel angiogenesis inhibitor and its target network. *Evid. Based Complement. Alternat. Med.* **2013**, 278405 (2013).
45. Zhang, B., Wang, X. & Li, S. An Integrative Platform of TCM Network Pharmacology and Its Application on a Herbal Formula, Qing-Luo-Yin. *Evid. Based Complement. Alternat. Med.* **2013**, 456747 (2013).
46. Paolini, G. V., Shapland, R. H., van Hoorn, W. P., Mason, J. S. & Hopkins, A. L. Global mapping of pharmacological space. *Nat. Biotechnol.* **24**, 805–815 (2006).
47. Hopkins, A. L. Network pharmacology: the next paradigm in drug discovery. *Nat. Chem. Biol.* **4**, 682–690 (2008).
48. Yildirim, M. A., Goh, K. I., Cusick, M. E., Barabasi, A. L. & Vidal, M. Drug-target network. *Nat. Biotechnol.* **25**, 1119–1126 (2007).
49. Ennis, H. L. & Lubin, M. Cycloheximide: Aspects of Inhibition of Protein Synthesis in Mammalian Cells. *Science* **146**, 1474–1476 (1964).
50. Nandi, R., Debnath, D. & Maiti, M. Interactions of berberine with poly(A) and tRNA. *Biochim. Biophys. Acta* **1049**, 339–342 (1990).
51. Khan, M. *et al.* Berberine and a Berberis lycium extract inactivate Cdc25A and induce alpha-tubulin acetylation that correlate with HL-60 cell cycle inhibition and apoptosis. *Mutat. Res.* **683**, 123–130 (2010).
52. Marcus, A. I. *et al.* The synergistic combination of the farnesyl transferase inhibitor lonafarnib and paclitaxel enhances tubulin acetylation and requires a functional tubulin deacetylase. *Cancer Res.* **65**, 3883–3893 (2005).
53. Piperno, G., LeDizet, M. & Chang, X. J. Microtubules containing acetylated alpha-tubulin in mammalian cells in culture. *J. Cell Biol.* **104**, 289–302 (1987).
54. Liu, Y. L. *et al.* Autophagy potentiates the anti-cancer effects of the histone deacetylase inhibitors in hepatocellular carcinoma. *Autophagy* **6**, 1057–1065 (2010).
55. Yang, P. M. *et al.* Inhibition of autophagy enhances anticancer effects of atorvastatin in digestive malignancies. *Cancer Res.* **70**, 7699–7709 (2010).
56. Yang, P. M. & Chen, C. C. Life or death? Autophagy in anticancer therapies with statins and histone deacetylase inhibitors. *Autophagy* **7**, 107–108 (2011).
57. Jones, K. R. *et al.* p53-Dependent accelerated senescence induced by ionizing radiation in breast tumour cells. *Int. J. Radiat. Biol.* **81**, 445–458 (2005).
58. Wang, N. *et al.* Berberine induces autophagic cell death and mitochondrial apoptosis in liver cancer cells: the cellular mechanism. *J. Cell. Biochem.* **111**, 1426–1436 (2010).
59. Yu, R. *et al.* Berberine-induced apoptotic and autophagic death of HepG2 cells requires AMPK activation. *Cancer Cell Int.* **14**, 49 (2014).

Acknowledgments

This work was supported by research grants from Taipei Medical University, Taipei Medical University Hospital, and Shuang Ho Hospital of Taiwan (TMU101-AE1-B25, TMU101-AE3-Y18 and 103TMU-SHH-02). The authors would like to thank the Office of Research and Development (Taipei Medicial University, Taipei, Taiwan) for the help in English editing.

Author contributions

P.-M.Y. designed and performed the majority of experiments and data analysis, as well as coordinated and drafted the manuscript. K.-H.L. participates in experimental designs and data analysis, and drafted the manuscript. H.-L.L. performed protein assays and the majority of western blot analyses. W.-C.T. performed wound-healing assays. H.H.H. performed western blot analyses. All authors read and approved the final manuscript.

Additional information

Supplementary information accompanies this paper at http://www.nature.com/scientificreports

Competing financial interests: The authors declare no competing financial interests.

How to cite this article: Lee, K.-H., Lo, H.-L., Tang, W.-C., Hsiao, H.H.-y. & Yang, P.-M. A gene expression signature-based approach reveals the mechanisms of action of the Chinese herbal medicine berberine. *Sci. Rep.* **4**, 6394; DOI:10.1038/srep06394 (2014).